ADVANCED MATERIALS INTERFACES
www.advmatinterfaces.de

Aramid Nanofiber Interphase for Enhanced Interfacial Shear Strength in Ultra-High Molecular Weight Polyethylene/Epoxy Composites

*Kelsey Steinke and Henry A. Sodano**

Ultra-high molecular weight polyethylene (UHMWPE) fibers are used in ballistic composites due to their high tenacity; unfortunately, their use in structural composites remains limited due to their poor adhesion with polymer matrix materials. Interphase design to the fiber surface is a promising approach to improve the interfacial properties of composite materials. This work describes the use of an aramid nanofiber (ANF) dip-coating treatment of plasma-treated UHMWPE fibers that increases surface roughness and enhances mechanical interlocking with the matrix. The ANFs also populate the fibers with polar functional groups, specifically hydroxyl, amide, ketone, and carboxyl, allowing for chemical bonding opportunities between the fiber and the epoxy matrix. The UHMWPE fiber surface chemical structure and composition is characterized using Fourier-transform infrared spectroscopy and X-ray photoelectron spectroscopy. The ANF dip-coating treatment yielded up to a 267% increase in fiber surface roughness, measured using atomic force microscopy. Using single fiber pullout testing, a maximum increase of 173% in interfacial shear strength is measured due to the ANF interphase, while completely maintaining the tensile strength of the fibers measured through single fiber tensile testing. These results demonstrate a simple and cost-efficient technique to improve the interfacial properties of UHMWPE composites through an ANF surface reinforcement.

1. Introduction

Fiber-reinforced polymer composites are materials of continuously increased importance in industries such as aerospace, automotive, sporting, and military applications. Ultra-high molecular weight polyethylene (UHMWPE) has found widespread use as a reinforcement in polymer matrix composites in many ballistic applications due to their desirable mechanical properties such as high modulus, low density, high energy absorption, excellent abrasion, and fatigue resistance.[1–3] Additionally, the non-polar, inert, and chemical resistant surface properties allowing the UHMWPE fibers to be biocompatible make them an attractive choice in many medical device applications. However, the inert surface chemistry severely hinders the performance of UHMWPE fiber-reinforced composites in structural applications.[4,5] The performance of composite materials is primarily dependent on the choice of fiber, matrix, and their final properties are typically dictated by the interface between them.[6] Interfacial properties in composite materials are usually determined by chemical interactions, mechanical interlocking, and the size of the surface area between both interface constituents.[7,8] Due to the previously mentioned smooth and chemically inert nature of the fiber surface, interfacial debonding is a common failure mode observed in UHMWPE composites when used in structural applications. The chemically inert surface of the fibers can also result in poor resin wetting of the fibers during composite manufacturing, which can lead to poor interfacial properties. Therefore, it is important to tailor the UHMWPE fiber-matrix interface so that the structural performance of composites can be improved, and their potential applications expanded.

To improve the fiber-matrix interface of UHMWPE fiber-reinforced polymer composites, researchers have primarily investigated fiber-surface treatments to produce reactive functional groups. Chromic acid[9–12] and corona discharge[13–16] treatments are methods that impart micro-pits and introduce functional groups onto the surface of the fibers to improve bonding with the matrix. However, chromic acid treatments and longer corona discharge treatment periods lead to a reduction in the strength of the fiber. Another series of studies have shown that plasma treatments can improve the fiber-matrix interface of UHMWPE fiber-reinforced composites through increasing fiber surface roughness and the introduction of polar functional groups, while preserving the tensile properties.[17–23]

K. Steinke, H. A. Sodano
Department of Materials Science and Engineering
University of Michigan
Ann Arbor, MI 48109, USA
E-mail: hsodano@umich.edu
H. A. Sodano
Department of Aerospace Engineering
University of Michigan
Ann Arbor, MI 48109, USA
H. A. Sodano
Department of Macromolecular Science and Engineering
University of Michigan
Ann Arbor, MI 48109, USA

The ORCID identification number(s) for the author(s) of this article can be found under https://doi.org/10.1002/admi.202102030.

DOI: 10.1002/admi.202102030

Wang et al. demonstrated the use of a tannic acid-Na^+ coating to introduce reactive functional groups onto the surface of UHMWPE fibers to improve the interfacial shear strength (IFSS) of the UHMWPE composites by 43.3%, compared to untreated composites.[24] Mohammadalipour et al. grafted glycidyl methacrylate (GMA) onto the UHMWPE fiber and embedded the fibers into a nano-clay/epoxy resin and demonstrated a 229% increase in IFSS measured using micro-droplet testing.[25] Ahmadi et al. determined that the addition of multi-walled carbon nanotubes to a GMA and amino-thiol chemical-treated fiber can yield a 336% improvement in IFSS.[26] Jin et al. coated plasma-treated UHMWPE fibers with polypyrrole and reported an 848% increase in compressive performance and a 54% increase in IFSS.[27]

An emerging nanoscale reinforcement has been aramid nanofibers (ANFs), which are obtained through the deprotonation and dissolution of macroscale aramid fibers in a dimethyl-sulfoxide/potassium hydroxide (DMSO/KOH) solution. During the deprotonation and dissolution process, intermolecular hydrogen bonds within the crystalline regions of the aramid fibers are cleaved, which yields ANFs of identical chemical and mechanical properties when compared to their macroscale counterparts, while also exhibiting superior surface reactivity.[28,29] ANFs are a promising nanofiller that have been incorporated into various polymer nanocomposites such that improvements in toughness, strength, and stiffness can be obtained.[30–33] Lin et al. isolated ANFs in the form of a powder, which were then dispersed into an epoxy matrix to study the ANFs impact on the mechanical performance of the resulting nanocomposites.[33] The reported results show that the ANFs were highly compatible with the epoxy matrix and yielded considerable improvements related to elastic properties and fracture toughness of the nanocomposites.[33] When the ANF reinforced epoxy resin was used to fabricate aramid laminates using vacuum-assisted resin transfer molding (VARTM), the short beam strength (SBS) improved by 43%, and Mode I fracture toughness improved by 17%.[34] Nasser et al. used a dip-coating method to directly assemble ANFs onto the surface of aramid fibers by means of physisorption and hydrogen bonding, which resulted in a 70.3% and 25.6% increase in IFSS and SBS, respectively.[35] A similar dip-coating process was used to directly assemble ANFs onto the surface of positively charged fiberglass through electrostatic adsorption, resulting in an 83.2% and 35.5% improvement in IFSS and SBS, respectively.[36] Park et al. used a layer-by-layer assembly approach to modify glass fibers with graphene oxide and ANFs, resulting in an IFSS increase of 39.2% when combined with an epoxy matrix.[37] By modifying the composition and architecture of the graphene oxide and ANF layers, the authors demonstrate the ability to tune the interfacial properties of glass fiber composites.[37] In the case of carbon fibers, Lee et al. used an electrophoretic deposition approach to assemble the ANFs onto the surface of the carbon fibers, which resulted in a 35% increase in IFSS.[38] The reported improvements in IFSS can be attributed to enhanced mechanical and chemical interactions between the fiber and the matrix due to the ANFs ability to increase both the roughness and chemical reactivity of the fiber surface. For this reason, ANFs have great potential as an interfacial reinforcement in UHMWPE composites.

In this work, the effectiveness of a simple dip-coating process for the assembly of an ANF interphase onto the surface of plasma-treated UHMWPE fibers is demonstrated. The chemical structure and composition of the ANF-coated fiber surface were characterized by Fourier-transform infrared spectroscopy (FTIR) and X-ray photoelectron spectroscopy (XPS). The UHMWPE surface morphology was characterized by scanning electron microscopy (SEM), and the surface roughness was measured by atomic force microscopy (AFM). The structural integrity of the treated fibers was assessed using single fiber tensile testing, while changes in interfacial properties due to the introduced ANF interphase were evaluated through single fiber pullout testing.

2. Experimental Section

2.1. ANF Surface Coating

UHMWPE plain-weave fabric (Spectra fabric style 932 received from Saati) was cleaned through successive 30 min sonication in 500 mL of acetone and ethanol. The cleaned fabric was then dried in an oven at 80 °C for 1 h. Following cleaning, the fabric was oxygen-plasma treated inside an SPI Plasma Prep II with an oxygen atmosphere (99.6% purity) for 30 s to introduce oxygen functional groups. Individual fibers were then removed from the woven fabric and partially attached to Teflon frames using 5-min epoxy, leaving one end of the fiber hanging free, as seen in **Figure 1**. An ANF (0.2 wt.%) solution was prepared according to the dissolution and deprotonation method described by Yang et al.[28] The ANF colloidal suspension was obtained by mixing 1.0 g of macroscale aramid fibers and 1.5 g of potassium hydroxide (KOH) in 500 mL of dimethylsulfoxide (DMSO), followed by stirring at 350 revolutions per min (rpm) at room temperature until the aramid fibers were completely dissolved. The solution was then poured into a 500 mL beaker and the Teflon frame was submerged in the beaker for treatment periods of 1-, 3-, 5-, and 7-min (Figure 1). Once the dip-coating process was completed, the fibers were rinsed in water and dried in a vacuum oven at 60 °C for 24 h.

2.2. ANF Surface Characterization

Following the ANF dip-coating process, the surface chemistry and morphology of the UHMWPE fibers were characterized using multiple techniques. To confirm the presence of ANFs and characterize the chemical structure of the ANF interphase on the surface of the UHMWPE fibers, FTIR was performed using a Nicolet iS60 spectrometer (Thermo Scientific) with a SMART diamond iTR accessory. The changes to the chemical composition of the fiber surface due to the introduced ANFs were characterized using XPS obtained from a Kratos axis ultra XPS. A broad spectra and C1s spectra were obtained and decomposed using CasaXPS software that utilized a Marquette regression function to create deconvoluted peaks of 70–30% Gaussian-Lorentzian distributions with the full-width, half max constrained to 0.8–1.7 eV. The ANF-coated UHMWPE fiber-surface morphologies were SEM imaged using a JEOL

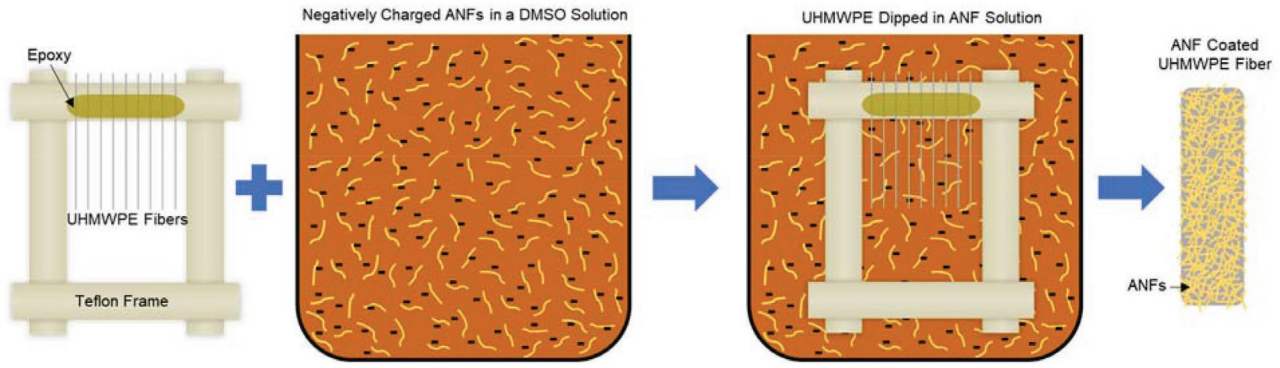

Figure 1. Schematic of the ANF dip-coating treatment process.

7800 FLV, while surface roughness was measured using a Park Systems XE-70 AFM in non-contact mode.

2.3. Mechanical Testing

To ensure the structural integrity of the UHMWPE fibers was not compromised during the ANF dip-coating process, single fiber tensile tests were performed according to ASTM C-1557. The ends of individual UHMWPE fibers were sandwiched between two 38 mm × 13 mm pieces of sandpaper using high shear strength epoxy (Loctite 9430 Hysol) cured at 82 °C for 1 h, such that a gauge length of 12.7 mm was attained (**Figure 2**A). The samples were then tested with a 5-N load cell on a 5982 Series Instron load frame at a rate of 0.05 mm s^{-1}. To avoid slippage during testing, alligator clips were used to clamp the tabs into place.

To evaluate the IFSS of the ANF-coated UHMWPE fibers, single fiber pullout tests were performed. Individual treated fibers were inserted into a slit of a silicon mold, where the embedded length was less than 300 µm, verified with an optical microscope.[39,40] The silicon molds were filled with an Epon 862 and Epikure 3230 epoxy mixture at a weight ratio of 100:35 and cured at 80 °C for 8 h. Following the curing process, the samples were removed from the silicon molds, and tabs were added to the free end of the fiber using the same Epon 862/Epikure 3230 resin mixture. After the resin mixture was applied for the tabs, the fiber was cured at 80 °C for 8 h. The single fiber pullout test was performed on a 5982 Series Instron frame equipped with a 5-N load cell at a rate of 0.016 mm s^{-1}. To avoid slippage during testing, alligator clips were used to clamp the tabs into place.

3. Results and Discussion

3.1. ANF Surface Coating and Characterization

FTIR was used to investigate changes in the chemical structure of the UHMWPE fiber surface post-plasma and ANF dip-coating treatments. FTIR was performed on the ANF-coated UHMWPE fibers with various treatment periods of 1-, 3-, 5-, and 7-min (**Figure 3**A). As seen in Figure 3B, the surface plasma treatment performed prior to the ANF-coating yields new oxygen-based functional groups at 1735 and 1110 cm^{-1}, which correspond to C=O and C−O−C, respectively.[41] The introduction of polar

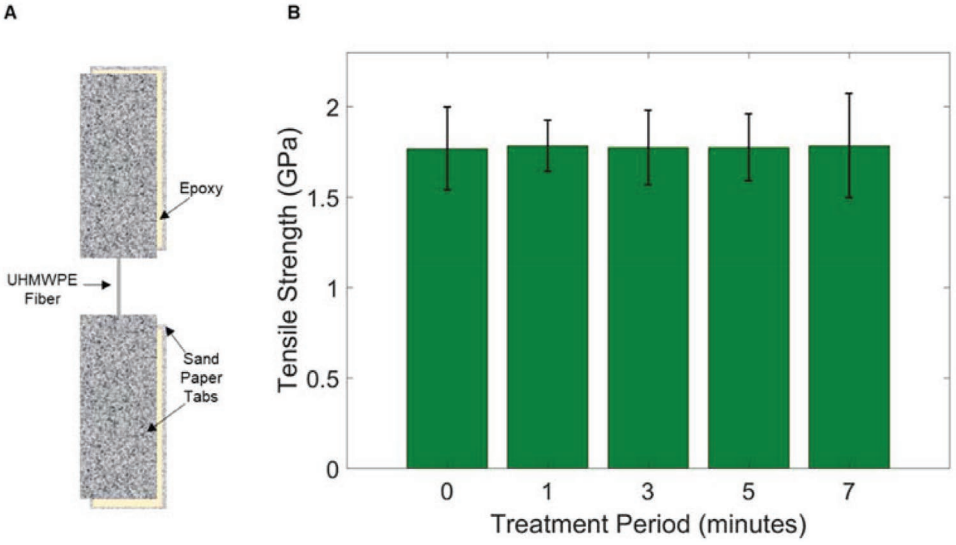

Figure 2. A) Schematic of a single UHMWPE fiber tensile test specimen. B) Tensile strength of untreated and ANF-coated UHMWPE single fibers.

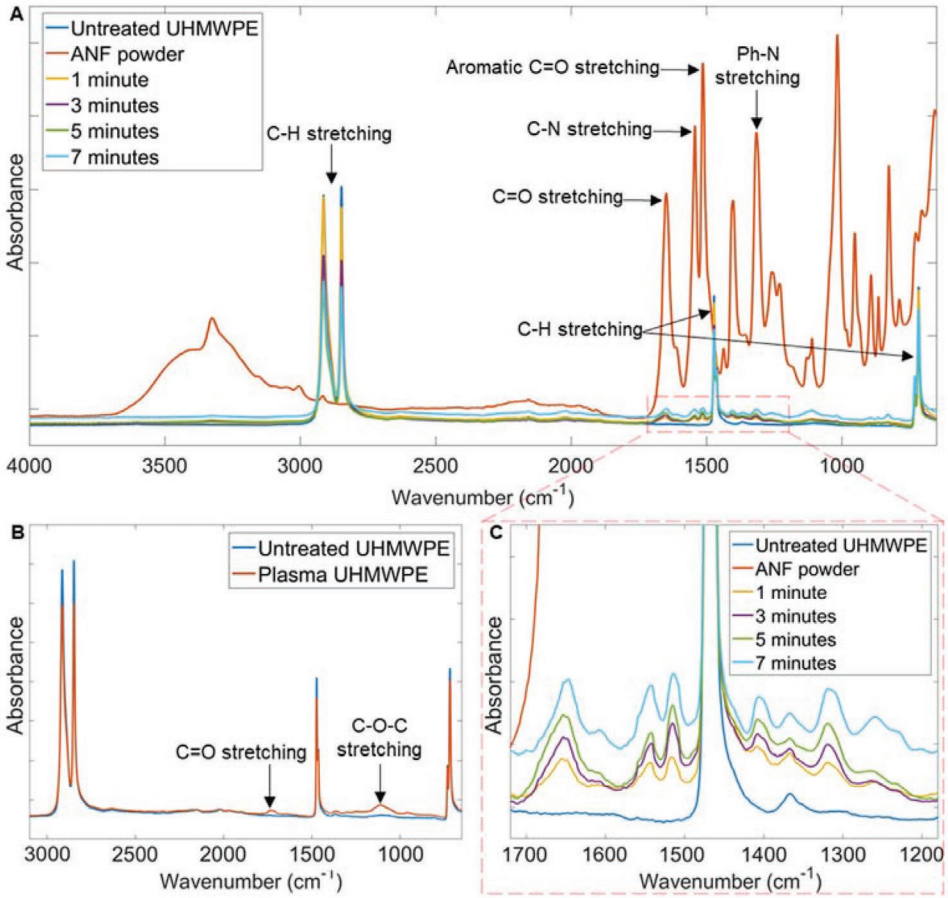

Figure 3. A) FTIR spectra of untreated UHMWPE, isolated ANFs, and ANF-coated UHMWPE fibers for various treatment periods fibers with corresponding peaks. B) FTIR spectra of untreated UHMWPE and 30 s plasma treated UHMWPE. C) FTIR spectra of untreated UHMWPE, isolated ANF, and ANF-coated UHMWPE fibers for various treatment periods with wavelengths ranging between 1715 and 1190 cm^{-1}.

oxygen functional groups on the originally inert UHMWPE fiber surface can enable and allow for a higher degree of chemical interaction through intermolecular forces, such as dipole-dipole interactions between the UHMWPE fiber and polar ANFs.[28,33,34] Once an ANF interphase is introduced, the FTIR spectra of the treated fibers display distinct ANF absorbance peaks which correspond to C=O stretching (1648 cm^{-1}), C—N stretching (1542 cm^{-1}), C=C stretching (1523 cm^{-1}), and Ph—N stretching (1316 cm^{-1}), irrespective of treatment periods (Figure 3A). In addition, all of the treated fibers display polyethylene absorbance peaks, which correspond to C—H stretching (2914, 2848, 1472, and 716 cm^{-1}). The results confirm that the dip-coating process successfully produces an ANF-coating on the fiber surface. The results also confirm the addition of polar functional groups on the surface of the UHMWPE fiber due to the ANFs, which have been previously demonstrated to be compatible with epoxy functional groups, therefore providing a mechanism to improve chemical interactions at the fiber-matrix interface.[33,34] It should be noted that no significant polyethylene absorbance peak shifts were observed, which confirms that the fiber treatment does not damage the fiber's chemical structure. When comparing the ANF dip-coating treatment period (Figure 3C), the absorbance peaks corresponding to C=O stretching, C—N stretching, C=C stretching, and Ph—N stretching are found to increase with increased soaking. The increase in absorbance peaks signals a correlation between the amount of ANFs introduced onto the fiber surfaces and treatment duration.

XPS analysis was used to further investigate the chemical composition of the UHMWPE surface following the plasma and ANF dip-coating processes. The XPS broad spectra concentrations of carbon, oxygen, and nitrogen of untreated, plasma-treated, ANF-coated UHMWPE for various treatment periods and ANF powder are shown in **Table 1**. From Table 1, it can be seen that post-oxygen plasma treatment, the UHMWPE fiber surface oxygen content was increased considerably from 6.41% to 15.2%. Once ANFs were introduced using a 1-min treatment, nitrogen concentration on UHMWPE fiber surfaces is found to increase from 0% to 5.05% up until matching that of ANF powder after a 7-min treatment. The introduced nitrogen on the UHMWPE surface can be attributed to the amide bonds that constitute aramid materials, thus confirming the presence of an ANF surface coating.

The normalized C1s XPS spectra of untreated UHMWPE, ANF-coated UHMWPE fibers for various treatment periods, and isolated ANF powder are shown in **Figure 4**. It can be seen in Figure 4 that the ANF-coated UHMWPE surface exhibits similar chemical composition peaks to that of the ANF powder,

Table 1. Broad XPS survey concentrations of overall carbon, nitrogen, and oxygen contents of untreated, oxygen-plasma treated, ANF-coated UHMWPE for various treatment periods and ANF powder.

UHMWPE fiber	C%	O%	N%
Untreated	93.59	6.41	0
Plasma treated	84.17	15.20	0
1 min	83.92	11.03	5.05
3 min	82.78	10.94	6.29
5 min	82.66	10.74	6.61
7 min	82.56	9.91	7.53
ANF Powder	81.29	9.97	8.74

confirming the presence of ANFs on the fiber surface. The C—C and C=O peaks decrease while the C—N and COOH peaks increase with increased treatment periods. After a 7-min treatment period, the C1s spectra are similar to the ANF powder, which is likely caused by the ANF-coating exceeding the interaction volume of XPS during the longer soak times. The decomposed C1s energy state concentrations of the ANF-coated fibers for various treatment periods can be seen in **Table 2**. The presence of oxygen functional groups on the fiber surface after the ANF treatment presents the potential to enhance the chemical interaction at the fiber-matrix interface.

SEM images were used to investigate the surface morphology of the UHMWPE fibers following ANF dip-coating. The ANF used in this work is reported to have diameters of 2–5 nm and lengths of 3–10 µm.[33,35,36,42] As seen in **Figure 5**A,B, the untreated fiber surface displays a smooth texture, which does not provide the opportunity for mechanical interlocking between the matrix and fiber. Following a one-min ANF dip-coating treatment, the fiber surface was found to display a rougher morphology due to adsorption of entangled ANFs (Figure 5C,D). As the treatment period is increased to 3-min, the ANF-coating was found to densify and completely cover the fiber surface, forming a complete ANF interphase. As seen in Figure 5G–J, once the treatment period is increased to 5-min or longer, signs of ANF surface agglomerations begin to appear, yielding non-uniform and porous coatings.

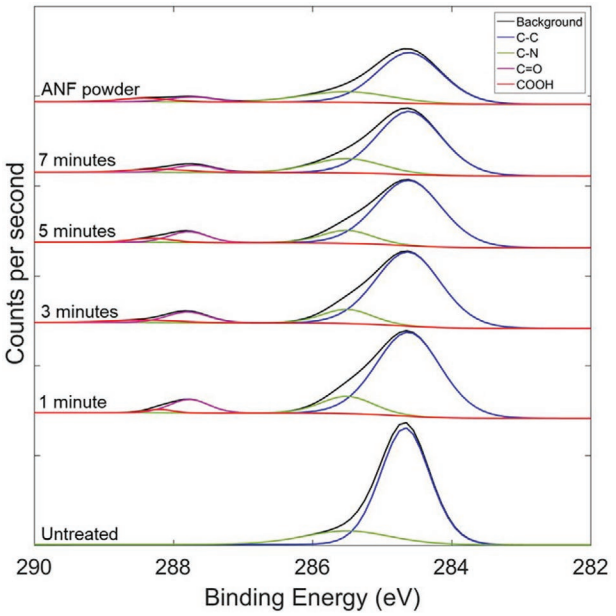

Figure 4. C1s XPS spectra of untreated UHMWPE, ANF-coated UHMWPE fibers for various treatment periods, and ANF powder, deconvoluted by existing carbon states.

The ANF-induced changes in surface morphology were also quantified using AFM characterization. In agreement with SEM imaging, **Figure 6** displays a significant increase in fiber surface roughness with increasing treatment periods. Both the root-mean square (RMS) (R_q) and the average roughness (R_a) of the fiber surface were measured using XEI (PSIA Corporation) analysis software (**Table 3**). Both R_q and R_a of ANF-coated UHMWPE fibers were found to increase with increasing treatment period, reaching a maximum increase of 267% and 227% after a treatment period of 7-min, respectively. The roughened UHMWPE surface due to the ANF-coating, shown through SEM imaging and AFM scanning, yields a larger interaction surface area between the fiber and matrix, and provides further opportunity for mechanical interlocking, which can contribute to strengthening the interfacial adhesion within UHMWPE composites.[35,36,38] The large increase in surface roughness seen after 5- and 7- min can signify the formation of agglomerations and a non-uniform surface which are expected to be undesirable since they can cause interfacial defects and voids that have the ability to reduce the interfacial strengthening effect of the proposed interphase.

3.2. Mechanical Testing

A critical component of any proposed fiber surface treatment is to ensure that the structural integrity of the fiber is not affected by the interfacial enhancement method. To confirm that the ANF dip-coating process does not degrade the mechanical strength of the UHMWPE fibers, single fiber tensile tests were performed. Due to the inert surface of the untreated fiber and the fiber's tendency to slip through the tabs during testing, a modified tensile testing method was used. As shown in Figure 2B the tensile strength of the untreated and ANF-coated fibers was found to have no statistical difference, regardless of treatment period. The lack of statistical difference is expected since the short dip-coating treatment period used in this study limits the exposure of the polymeric fibers to the basic ANF/DMSO solution and avoids damaging the fibers due to chemical exposure. The conservation of the tensile properties in the

Table 2. XPS decomposed C1s energy state concentrations for ANF-coated UHMWPE fibers for various treatment periods compared to isolated ANF powder.

Treatment periods [min]	C—C%	C—N%	C=O%	COOH%
1	78.31	13.03	7.47	1.18
3	78.53	11.44	7.24	2.79
5	77.66	11.89	7.55	2.90
7	73.53	17.93	5.25	3.20
ANF powder	71.51	20.00	4.68	3.82

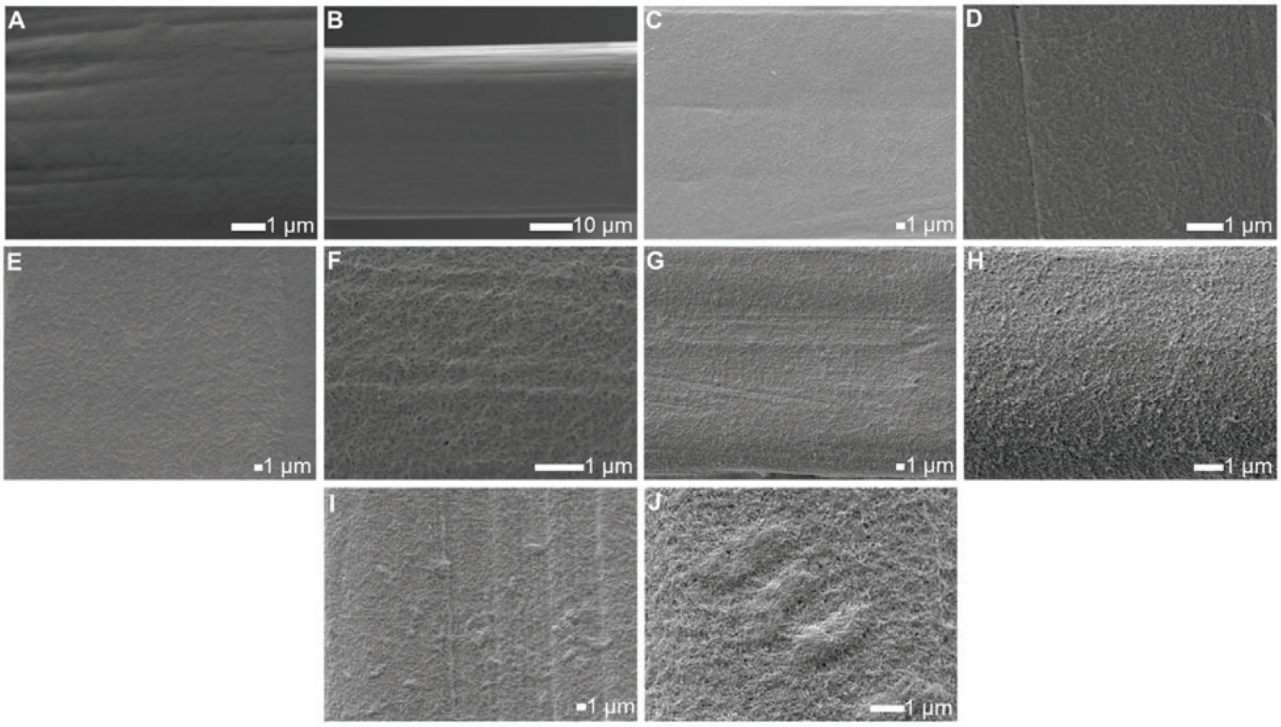

Figure 5. SEM images of untreated UHMWPE and ANF-coated UHMWPE fiber surfaces for varying treatment periods. A,B) Untreated UHMWPE fiber surface. C,D) 1-min treatment period. E,F) 3-min treatment period. G,H) 5-min treatment period. I,J) 7-min treatment period.

fibers following ANF dip treatment is consistent with previously reported studies.[35,36,43]

Given the importance of interfacial adhesion to the overall performance of composite materials, single fiber pullout testing was performed to evaluate the IFSS of the ANF-coated UHMWPE fibers. Pullout testing allows the direct measurement of the interfacial debonding force between an individual fiber and the matrix.[44,45] The advantages of

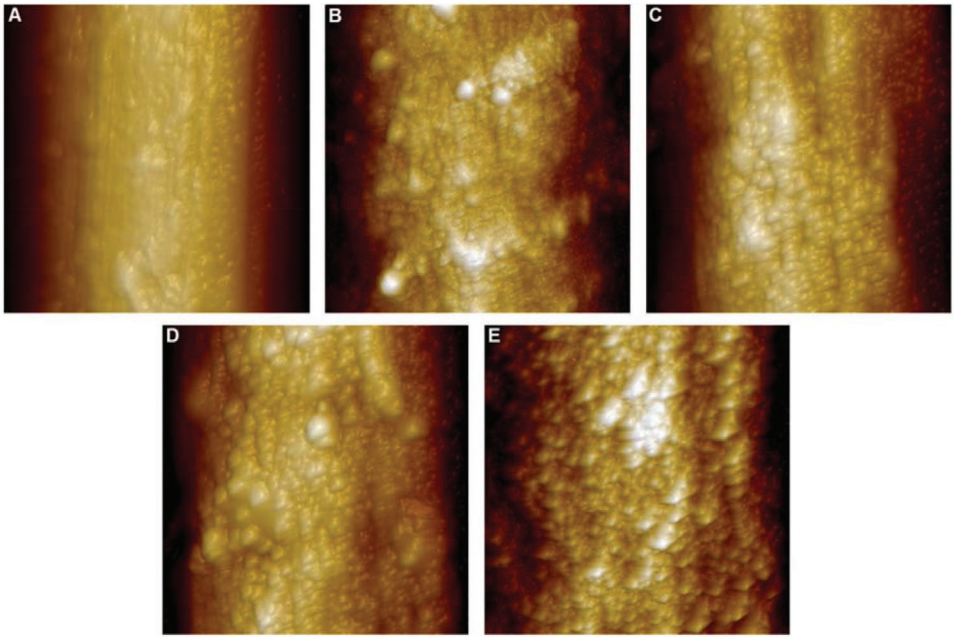

Figure 6. Non-contact surface AFM scans of untreated and ANF-coated UHMWPE fiber surfaces. A) Untreated, B) 1-min, C) 3-min, D) 5-min, and E) 7-min.

Table 3. Measured RMS Rq and Ra of untreated UHMWPE and ANF-coated UHMWPE with varying dip-coating treatment periods.

Treatment period [min]	R_q [nm]	R_a [nm]
Untreated	12	11
1	19	15
3	27	24
5	37	32
7	44	36

single fiber pullout testing over other techniques (e.g., single fiber segmentation, micro-droplet, and fiber pushout) are the test's low-data variability, ease of specimen fabrication, interfacial failure mode control potential, and the compatibility with both polymer and ceramic fibers.[44,45] Neat and ANF-coated fibers were embedded in an epoxy matrix before a large epoxy tab was attached to the free end of the fiber. Once the tab was attached, the fibers were mounted in an Instron load frame, as seen in **Figure 7**A. Large epoxy tabs were used so that the tabs could be sufficiently gripped and to ensure fiber pull out before slipping in the tab could occur. It should be noted that if slipping was observed, the data was deemed invalid and excluded from the results. The measured IFSS of untreated and ANF-coated fibers are shown in Figure 7B and after only a 1-min treatment, the ANF-coated fibers (6.97 MPa) displayed a 123% increase in IFSS relative to untreated fibers (3.12 MPa). Interfacial adhesion was further improved after a 3-min treatment, where a 173% increase in the IFSS of ANF-coated fibers (8.51 MPa) was measured, relative to untreated fibers. The increased fiber surface roughness due to the ANFs coating allows for the fiber to be firmly embedded into the epoxy matrix, increasing interfacial surface area and enhancing the mechanical interlocking mechanism between the fiber and the matrix. By hierarchically nano-structuring the fiber-matrix interface, the ANF interphase contributed to a reduction in interfacial stress concentration and an improvement in load transfer between the typically smooth fiber and epoxy matrix. As the treatment period was increased to 5- and 7-min, the IFSS of the ANF-coated fibers experienced an 11% and 20% decrease in IFSS, respectively, relative to those samples treated for 3-min. This decrease can be attributed to a non-uniform and porous coating, as well as the formation of ANF agglomerations on the fiber surface (Figure 5G–J). Such fiber surface characteristics can increase the density of defects at the interface and act as site for failure initiation, thus introducing discontinuity within the interfacial region and ultimately yielding a lower IFSS in UHMWPE composites.[36,38] It should be noted that, irrespective of the treatment period, the IFSS was substantially increased relative to untreated fibers. The ANF interphase promoted a greater degree of chemical bonding between the typically inert UHMWPE surface and the epoxy matrix. The chemical interaction between the ANFs polar functional groups and the polar groups found in the epoxy matrix was enabled, which allowed for improved surface wetting and chemical bonding between the ANF-coated fibers and the epoxy matrix. The contact angle of epoxy droplets on untreated, plasma-treated, and ANF-coated UHMWPE fibers for various treatment periods of 1-, 3-, 5-, and 7-min were measured. The contact angle measurements (Table S1, Supporting Information) demonstrate that the low surface energy of UHMWPE is overcome and the surface polarity is modified and increases post-plasma and ANF-coating treatment. The IFSS results show that the use of a dip-coating method to introduce an ANF interphase on the surface of UHMWPE fibers is an effective method to improve interfacial adhesion in the fiber's corresponding epoxy matrix composites.

Post-pullout SEM images were taken to further understand the interfacial failure mechanism where the UHMWPE fibers displayed a smooth, clean, and ANF-free surface (**Figure 8**). As seen in Figure 5, the fiber surfaces were originally coated with an entangled ANF interphase that provided a roughened surface morphology. Due to the larger interaction area between the ANFs and the epoxy matrix when compared to the ANFs and the fiber, the ANFs debonded from the fiber surface and remained embedded in the epoxy matrix. Therefore, the resulting interfacial failure is observed at the ANF-UHMWPE fiber interphase.

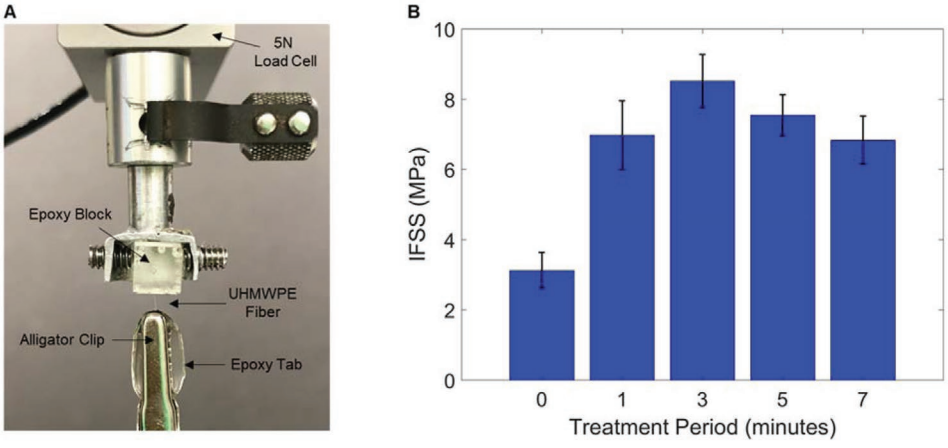

Figure 7. A) Single UHMWPE fiber pullout experimental setup. B) IFSS of untreated and ANF-coated UHMWPE fibers for various treatment periods.

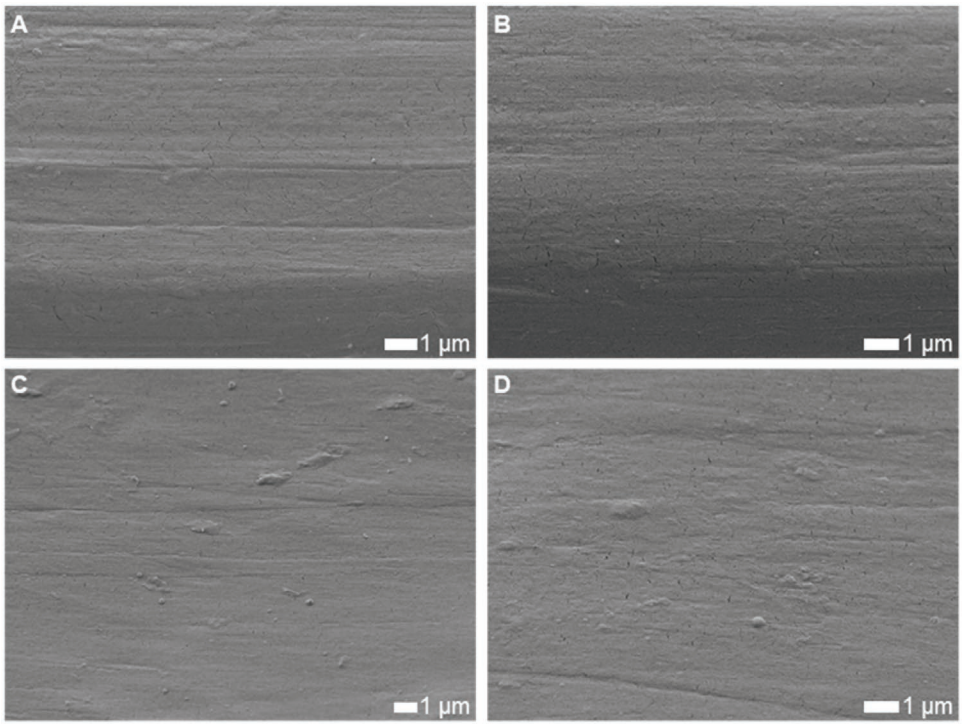

Figure 8. SEM images of deboned ANF-coated UHMWPE fiber surfaces after single fiber pullout testing. A) 1-min treatment period. B) 3-min treatment period. C) 5-min treatment period. D) 7-min treatment period.

4. Conclusion

This study presents a straightforward and rapid method to introduce ANFs onto the surface of UHMWPE fibers, which improves the fiber's interfacial adhesion with the epoxy matrix. Uniform and well-adhered ANF-coatings were introduced on the surface of plasma-treated fibers using a short dip-coating process. As the dip-coating treatment period increased, the concentration of ANFs on the surface of the fiber also increased providing a nanostructured interphase with greater polar functional groups to improve resin wetting and chemical interaction between the fiber and epoxy matrix. The ANF interphases also yielded greater surface roughness, increasing RMS R_q by a minimum of 58% relative to untreated fibers, therefore providing a much-needed mechanical interlocking mechanism between the originally smooth UHMWPE fiber surface and epoxy matrix. The ANF-coating was found to increase the interfacial shear strength by more than 100%, irrespective of treatment period, with a maximum improvement of 173% after soaking for 3 min. The process was shown to preserve the tensile strength of the fibers, therefore, avoiding trade-offs between the interfacial improvement and the in-plane strength of UHMWPE composite materials. This work has shown that an ANF-coating has the potential to be integrated into the continuous production of high-performance UHMWPE fiber-reinforced composites.

Supporting Information

Supporting Information is available from the Wiley Online Library or from the author.

Acknowledgements

The authors gratefully acknowledge financial support for this research from the Air Force Office of Scientific Research under Contract # FA9550-21-1-0019 and the Army Research Office under Contract # W911NF-18-1-0061.

Conflict of Interest

The authors declare no conflict of interest.

Data Availability Statement

Research data are not shared.

Keywords

aramid nanofibers, interfacial shear strength, nanostructured interphase, single fiber pullout, ultra-high molecular weight polyethylene fibers

Received: October 17, 2021
Revised: December 17, 2021
Published online: January 29, 2022

[1] T. Tam, A. Bhatnagar, *Lightweight Ballistic Composites Military and Law-Enforcement Applications*, Elsevier, Cambridge, MA **2006**.
[2] P. Bajaj, Sriram, *Indian J. Fibre Text. Res.* **1997**, *22*, 274.
[3] M. Vlasblom, *Handbook of Properties of Textile and Technical Fibres*, Elsevier, Cambridge, MA **2018**.

[4] J. L. Holloway, A. M. Lowman, M. R. VanLandingham, G. R. Palmese, *Compos. Sci. Technol.* **2013**, *85*, 118.
[5] A. P. Kharitonov, A. V. Maksimkin, K. S. Mostovaya, S. D. Kaloshkin, M. V. Gorshenkov, T. P. D'yachkova, A. G. Tkachev, L. N. Alekseiko, *Compos. Sci. Technol.* **2015**, *120*, 26.
[6] K. K. Chawla, *Composite Materials: Science and Engineering*, Springer, New York **2012**.
[7] M. R. Wisnom, *Philos. Trans. R. Soc., A* **2012**, *370*, 1850.
[8] N. J. Pagano, G. A. Schoeppner, *Comprehensive Composite. Materials*, Elsevier, Cambridge, MA **2000**.
[9] W. Li, L. Meng, R. Ma, *Polym. Test.* **2016**, *55*, 10.
[10] Y. Muraoka, M. J. Rich, L. T. Drzal, *J. Adhes. Sci. Technol.* **2012**, *16*, 1669.
[11] M. S. Silverstein, O. Breuer, *J. Mater. Sci.* **1993**, *28*, 4153.
[12] W. Li, R. Li, C. Li, Z.-R. Chen, L. Zhang, *Polym. Compos.* **2017**, *38*, 1215.
[13] N. Bahramian, M. Atai, M. R. Naimi-Jamal, *Dent. Mater.* **2015**, *31*, 1022.
[14] T. Ogawa, H. Mukai, S. Osawa, *J. Appl. Polym. Sci.* **1999**, *71*, 243.
[15] T. Ogawa, H. Mukai, S. Osawa, *J. Appl. Polym. Sci.* **2001**, *79*, 1162.
[16] W. S. Gutowski, E. R. Pankevicius, *Compos. Interfaces* **1993**, *1*, 141.
[17] S. I. Moon, J. Jang, *J. Mater. Sci.* **1998**, *33*, 3419.
[18] S. I. Moon, J. Jang, *Compos. Sci. Technol.* **1999**, *59*, 487.
[19] B. Tissington, G. Pollard, I. M. Ward, *J. Mater. Sci.* **1991**, *26*, 82.
[20] P. Masse, J. P. Cavrot, P. François, J. M. Lefebvre, B. Escaig, *Polym. Compos.* **1994**, *15*, 247.
[21] S. G. Lee, T. J. Kang, T. H. Yoon, *J. Adhes. Sci. Technol.* **1998**, *12*, 731.
[22] Y. F. Fu, K. Xu, J. Li, Z. Y. Sun, F. Q. Zhang, D. M. Chen, *Polym.-Plast. Technol. Mater.* **2012**, *51*, 273.
[23] R. He, F. Niu, Q. Chang, *Surf. Interface Anal.* **2018**, *50*, 73.
[24] S. Wang, J. Ma, X. Feng, J. Cheng, X. Ma, Y. Zhao, L. Chen, *Polym. Compos.* **2020**, *41*, 1614.
[25] M. Mohammadalipour, M. Masoomi, M. Ahmadi, S. Safi, *RSC Adv.* **2016**, *6*, 41793.
[26] M. Ahmadi, O. Zabihi, M. Masoomi, M. Naebe, *Compos. Sci. Technol.* **2016**, *134*, 1.
[27] X. Jin, W. Wang, C. Xiao, T. Lin, L. Bian, P. Hauser, *Compos. Sci. Technol.* **2016**, *128*, 169.
[28] M. Yang, K. Cao, L. Sui, Y. Qi, J. Zhu, A. Waas, E. M. Arruda, J. Kieffer, M. D. Thouless, N. A. Kotov, *ACS Nano* **2011**, *5*, 6945.
[29] K. Cao, C. P. Siepermann, M. Yang, A. M. Waas, N. A. Kotov, M. D. Thouless, E. M. Arruda, *Adv. Funct. Mater.* **2013**, *23*, 2072.
[30] S. A. Park, Y. Eom, H. Jeon, J. M. Koo, T. Kim, J. Jeon, M. J. Park, S. Y. Hwang, B. S. Kim, D. X. Oh, J. Park, *ACS Macro Lett.* **2020**, *9*, 558.
[31] J. M. Koo, H. Kim, M. Lee, S. A. Park, H. Jeon, S. H. Shin, S. M. Kim, H. G. Cha, J. Jegal, B. S. Kim, B. G. Choi, S. Y. Hwang, D. X. Oh, J. Park, *Macromolecules* **2019**, *52*, 923.
[32] J. Zhu, W. Cao, M. Yue, Y. Hou, J. Han, M. Yang, *ACS Nano* **2015**, *9*, 2489.
[33] J. Lin, S. H. Bang, M. H. Malakooti, H. A. Sodano, *ACS Appl. Mater. Interfaces* **2017**, *9*, 11167.
[34] B. A. Patterson, M. H. Malakooti, J. Lin, A. Okorom, H. A. Sodano, *Compos. Sci. Technol.* **2018**, *161*, 92.
[35] J. Nasser, J. Lin, K. Steinke, H. A. Sodano, *Compos. Sci. Technol.* **2019**, *174*, 125.
[36] J. Nasser, K. Steinke, L. Zhang, H. Sodano, *Compos. Sci. Technol.* **2020**, *192*, 108109.
[37] B. Park, W. Lee, E. Lee, S. H. Min, B. S. Kim, *ACS Appl. Mater. Interfaces* **2015**, *7*, 3329.
[38] J. U. Lee, B. Park, B. S. Kim, D. R. Bae, W. Lee, *Composites, Part A* **2016**, *84*, 482.
[39] H. S. Hwang, J. Nasser, H. A. Sodano, *Exp. Mech.* **2019**, *59*, 979.
[40] J. Nasser, J. Lin, H. Sodano, *J. Appl. Phys.* **2018**, *124*, 045305.
[41] M. R. Sanchis, V. Blanes, M. Blanes, D. Garcia, R. Balart, *Eur. Polym. J.* **2006**, *42*, 1558.
[42] J. Nasser, L. Zhang, J. Lin, H. Sodano, *ACS Appl. Polym. Mater.* **2020**, *2*, 2934.
[43] J. Nasser, L. Zhang, H. Sodano, *Composites, Part B* **2020**, *197*, 108130.
[44] C. DiFrancia, T. C. Ward, R. O. Claus, *Composites, Part A* **1996**, *27*, 597.
[45] B. F. Sørensen, H. Lilholt, *IOP Conf. Ser.: Mater. Sci. Eng.* **2016**, *129*, 012009.